J. Fluid Mech. (2002), *vol.* 460, *pp.* 337–348.
DOI: 10.1017/S0022112002008212 Printed in the United Kingdom

Surface folds during the penetration of a viscoelastic fluid by a sphere

By THOMAS PODGORSKI AND ANDREW BELMONTE

The W. G. Pritchard Laboratories, Department of Mathematics, Pennsylvania State University, University Park, PA 16802, USA

(Received 17 July 2001 and in revised form 16 January 2002)

When a sphere settles through the free surface of a viscous fluid, the interface is deformed and assumes a funnel shape behind the sphere. If the fluid is viscoelastic and the settling process is fast compared to the relaxation time of the fluid, elastic effects are dominant and an instability occurs. The interface loses its original axisymmetry and buckles, leading to a particular mode of pinch-off unseen in Newtonian fluids. We present experimental evidence that stress boundary layers form in this type of flow, and argue that a physical mechanism for this instability can be recovered, at least qualitatively, by considering the stability of a stretched anisotropic elastic membrane in a pressure field.

1. Introduction

When fluid properties depart from the linear (Newtonian) relationship between stress and strain rates, unusual phenomena can occur which are a challenge to common intuition. Simple experiments with viscoelastic fluids exhibit new behaviours unseen in their Newtonian counterparts such as the rod-climbing effect (Bird, Armstrong & Hassager 1987), elastic turbulence at low Reynolds number (Groisman & Steinberg 2000) or the apparent cusp at the trailing end of a rising bubble (Hassager 1979; Bird *et al.* 1987; Liu, Liao & Joseph 1995).

The example of the cusped bubble is particularly interesting because it involves an instability leading to symmetry breaking of the interface: the cusp assumes a striking knife-edge shape, as can be seen when observing a bubble rising in any commercial shampoo bottle turned upside-down. Jeong & Moffatt (1992) made a detailed calculation of the shape of bidimensional free-surface cusps in Newtonian fluids, and Liu *et al.* (1995) reported experiments on cusped bubbles in viscoelastic fluids, arguing that the same analytical profile could describe the locally bidimensional cusp shape. However, the mechanism leading to the loss of bubble axisymmetry and the cusp formation is not yet understood. Similar instabilities are also present in filament stretching, where a rapidly stretched viscoelastic filament loses axisymmetry, leading to a break-up process unseen in Newtonian fluids (Spiegelberg & McKinley 1996). Kumar & Graham (2000) showed that purely elastic buckling instabilities could explain some phenomena observed in contracting flows of viscoelastic liquids, and suggested that similar instabilities could be responsible for the bidimensional character of cusped bubbles.

In this paper, we present an experiment with viscoelastic fluids, in which a buckling instability could also be occurring. When a solid sphere is gently released on the free surface of a viscoelastic fluid, it pulls the interface down as it is settling. The

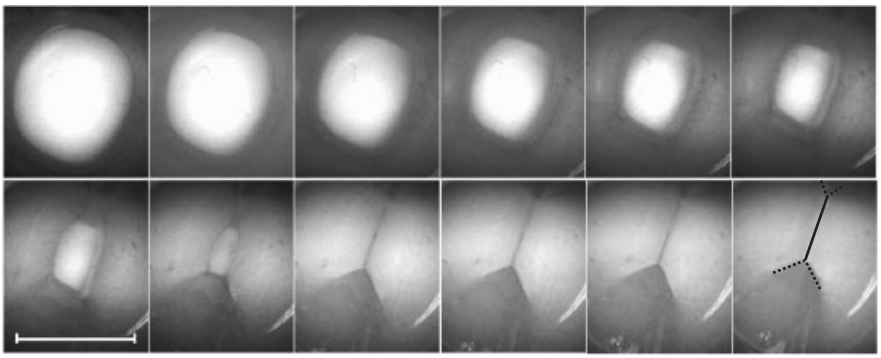

FIGURE 1. Temporal sequence of the settling of a sphere through a viscoelastic fluid surface, viewed from above. Interval between pictures: 1 s. In the last frame, dark lines were superimposed (see text). The bar gives the scale (1 cm).

deformed interface is initially axisymmetric and forms a funnel above the sphere, until an instability develops which leads to a loss of axisymmetry and the formation of a cusp when the interface pinches off. After the pinch-off, the cusp slowly relaxes, appearing as creases on the flat surface when observed from above. In contrast, the symmetry breaking is not observed in Newtonian fluids. This phenomenon is also observed when plunging vertically a cylindrical rod in a viscoelastic fluid (radial streaks develop around the rod), or more simply when mixing the solution with a magnetic stirrer or even a spoon.

We suggest a simple physical mechanism for the instability leading to the formation of non-axisymmetric cusps in the sphere settling experiment. Following the theoretical and numerical work of Kumar & Graham (2000) and numerical computations by Yao & McKinley (1998) and Rasmussen & Hassager (1999) suggesting that interfacial stress boundary layers could form in extensional interfacial flows of viscoelastic fluids, we present experimental evidence of their existence. Based on this we make a simplified treatment of the problem using a membrane model which leads to a qualitative interpretation of the phenomenon.

2. Experimental observations

We made an experimental study of the settling of rigid spheres through a viscoelastic fluid. For a qualitative exploration of the phenomena, spheres were gently released on the surface of a fluid placed in a cylindrical container, providing axisymmetric boundary conditions. An example is shown in figure 1 for a 3/4 in. teflon sphere slowly sinking in a micellar fluid described below. As clearly seen in this figure, the interface progressively loses axisymmetry and closes up forming a cusp. This cusp appears as a central crease on the surface (long black continuous line on the last picture of figure 1), with possible secondary creases (dotted lines) at both ends. In a cylindrical container, the orientation of the main crease is random, and different modes of instability can be observed, leading to various surface patterns shown in figure 2.

For more reproducible results and quantitative measurements, non-axisymmetric boundary conditions were used in order to select a particular mode of instability and its orientation with respect to the observer. The experimental setup is sketched in figure 3. The fluid lies in a rectangular Plexiglas container (length 15 cm, width

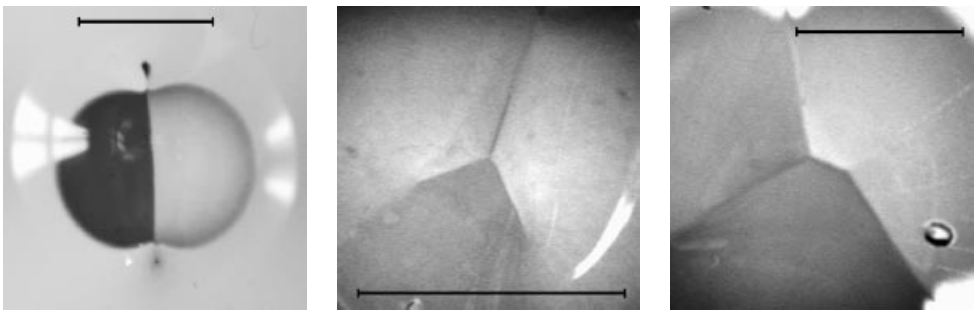

FIGURE 2. Surface folds resulting from different modes of instability. From left to right: mode 2, mode 3, and a mode 2 with secondary creases. The bar represents 1 cm on each image.

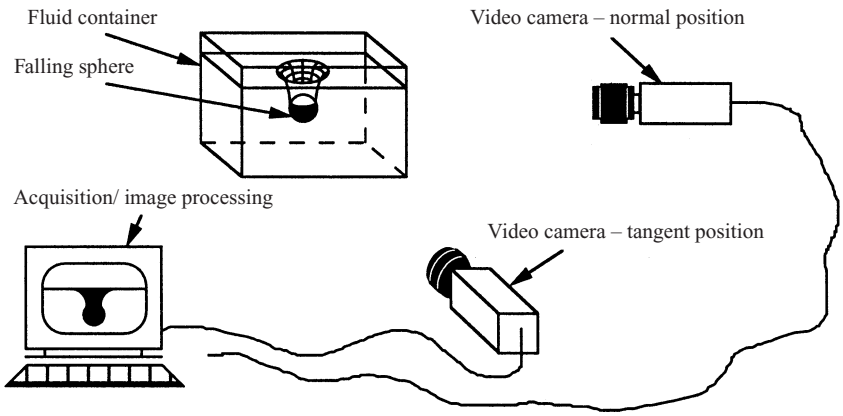

FIGURE 3. Experimental set-up.

6 cm, height 10 cm). The sphere is held half-immersed on the surface of the fluid with tweezers, and released with no initial velocity. Then it starts sinking in the fluid, deforming the interface, and the phenomenon is recorded with a video camera (COHU 4912) and a digital image processing system. The camera is placed along any of the three axes of the container.

With these boundary conditions, the system always selects an order-2 mode of instability, resulting in a single crease on the surface as shown on the first picture in figure 2, and its orientation is always parallel to the smallest side of the container. The interface folds more easily in this direction because the relative elongation and the associated elastic stress is smaller in the longest dimension. We refer to the direction perpendicular to the largest side of the box as the *tangent direction* (parallel to the cusp direction), and the direction perpendicular to the smallest side of the box as *normal direction* (normal to the cusp) (see figure 3).

We used spheres of diameters ranging from 3/8 in. (0.95 cm) to 1 in. (2.54 cm), and densities of $1.34\,\mathrm{g\,cm^{-3}}$ (Delrin) and $2.3\,\mathrm{g\,cm^{-3}}$ (Teflon). The fluid is a solution of cetylpyridinium chloride (CPCl) and sodium salicylate (NaSal), with respective molar concentrations of 100 mM and 60 mM. CPCl is a surfactant that is capable of forming long worm-like micelles in the presence of NaSal (Rehage & Hoffmann 1991). The fluid density is $\rho = 1.0\,\mathrm{g\,cm^{-3}}$. The strong viscoelastic properties of this fluid were measured in a Couette geometry with a Rheometrics RFS III rheometer at $T = 21\,^{\circ}\mathrm{C}$. For a typical strain rate $\dot{\gamma}$ (or frequency) of $0.1\,\mathrm{s^{-1}}$, the steady shear viscosity is

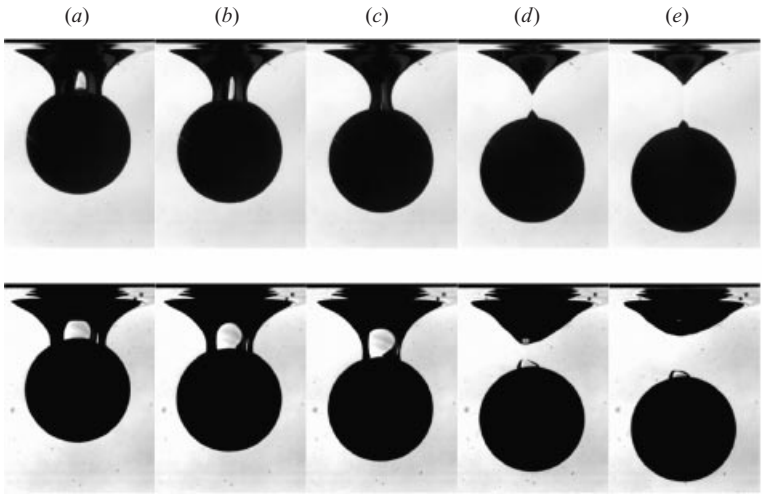

FIGURE 4. Temporal sequence of a 3/4 in. Teflon sphere settling through an aqueous solution of CPCl/NaSal (100 mM/60 mM). Top: tangent view; bottom: normal view. Interval between pictures is 1 s. Frame (*d*) corresponds to pinch-off time t_p.

$\eta = 140$ Pa s, and the dynamic storage and loss moduli are approximately equal ($G' \simeq G'' \simeq 30$ Pa). The relaxation time is estimated as $\lambda \simeq 6$ s from strain relaxation measurements. Thus in our experiments where the velocity is $U \sim 1\,\mathrm{mm\,s^{-1}}$ and the length scale a few millimetres (sphere radius R), the Deborah number $De = \lambda U/R$ is of order 1 and the Reynolds number is very low (typically 10^{-3}). Though the conditions are less ideal, the instability has also been observed in standard polymer solutions (carboxy-methyl-cellulose and poly-ethylene oxide).

Figure 4 shows a typical development of the instability. Initially, tangent and normal views are very similar, indicating an axisymmetric profile of the interface, with circular horizontal cross-sections, until at some point the interface loses axisymmetry when the width in the tangent view w_T becomes smaller than the width in the normal view w_N. As the width of the funnel decreases much faster in one direction, the interface eventually pinches off forming a bidimensional cusp that relaxes to the surface.

Since horizontal cross-sections of the interface are roughly elliptic, we characterize the asymmetry by the eccentricity, a function of the vertical coordinate z:

$$\varepsilon(z) = (w_N(z) - w_T(z))/(w_N(z) + w_T(z)). \tag{2.1}$$

At a given time t, $\varepsilon(z)$ is very small near the unperturbed free surface (at $z = 0$), and increases up to a maximum $\varepsilon_{max}(t)$ located roughly where the interface section reaches its smallest size. Below this point, the eccentricity decreases and drops to zero at the sphere (figure 5*a*). As the sphere settles, $\varepsilon_{max}(t)$ increases and the position of this maximum moves down with the sphere. Figure 5(*b*) shows the value of ε_{max} versus time for different experiments. The existence of a threshold for the instability is clearly visible on this figure. The eccentricity remains low for a long time and only increases slowly. At a critical time, when the interface has been sufficiently stretched, $\varepsilon_{max}(t)$ starts increasing faster, showing the rapid development of the instability. Figure 5(*b*) also reveals that the instability is more pronounced for big heavy spheres than for small light spheres; in the latter case, the time of the experiment is much longer than the relaxation time of the fluid.

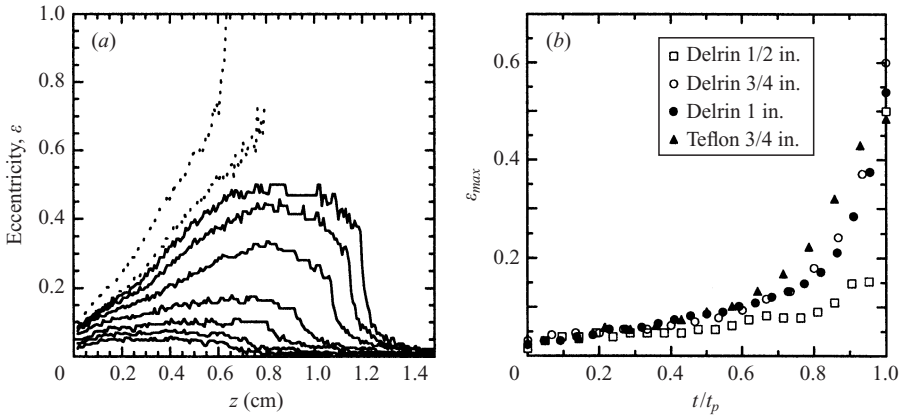

FIGURE 5. Experimental measurements of interface eccentricity $\varepsilon(z)$. (*a*) Temporal evolution of the eccentricity profile for a 3/4 in. Teflon sphere settling through an aqueous solution of CPCl/NaSal (100 mM/60 mM). From bottom to top, curves correspond to $t - t_p = -5$, -4, -3, -2, -1, -0.5, -0.1, 0.1 and 1 s, where t_p is the pinch-off time. Dotted curves are after pinch-off. (*b*) Position of the maximum eccentricity versus time for different spheres settling through the same micellar solution.

3. Stress boundary layers

Before attempting to model the instability discussed above, we made a qualitative visual observation of particle displacements in the fluid near the settling sphere. This visualization reveals a strong stretching flow in the vicinity of the free surface, whereas velocities and strains are relatively small elsewhere. We thus suspect that an extensional stress boundary layer occurs at the interface, which can be viewed as a natural consequence of the boundary conditions at the free surface: when an interface is pinned on two separating solid surfaces (the sphere and the walls of the container), its surface area must increase with time, which in our case is realized by a local stretching flow. Yao & McKinley (1998), Rasmussen & Hassager (1999) and Kumar & Graham (2000) have shown by different theoretical and computational means that stress boundary layers can form in extensional flows of viscoelastic fluids. However, their results all deal with specific models of viscoelastic fluids, namely the upper convected Maxwell (UCM) and Oldroyd-B models; they were not checked experimentally.

Worm-like micellar solutions are known to exhibit strong birefringent properties under flow (Hu, Wang & Jamieson 1993). As a consequence, when observed through crossed polarizers, one can readily see the distribution of stress, as in the popular photoelasticity technique used for solids. We performed a qualitative visualization of the stresses in a quasi-bidimensional flow where the interface is stretched in a similar way to the sphere experiment; the axisymmetric flow was less easy to visualize via birefringence techniques. We used a cell of width 15 cm, thickness 3.5 cm and height 30 cm filled with our fluid (100 mM CPCl, 60 mM NaSal). This cell was placed between two crossed linear polarizers as shown in figure 6(*a*), and lit from behind with a uniform source of light. When the fluid is at rest, it is optically isotropic and no light comes through the system. When a 0.2 cm thick and 3 cm wide plate is plunged vertically in the fluid at a constant speed of about 0.5 cm s^{-1}, the fluid is highly stretched both at the free liquid–air boundary and at the surface of the plate; it becomes strongly birefringent there. As visible from the closely spaced light and dark regions in figure 6(*b*), strong stress gradients occur in a thin boundary layer

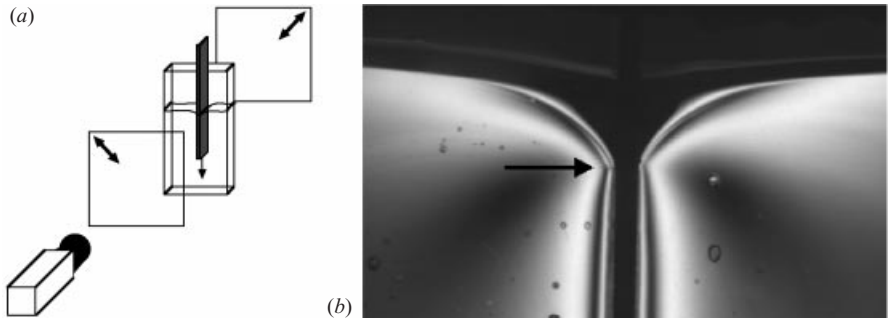

FIGURE 6. Visualization of stress boundary layers in a bidimensional flow using birefringence. (*a*) Set-up: the cell containing the fluid is placed between crossed linear polarizers (arrows indicate the axis of the polarizers); (*b*) Image obtained when a 2 mm thick plate plunges into the fluid at a velocity of about 0.5 cm s^{-1}. Fringes are seen where a concentration of stress occurs. The thickness of the plate sets the scale, and the arrow indicates the point of contact between the free surface and the plate.

which is only a few millimetres thick, whereas the stresses are more uniform and much smaller in the bulk. It is reasonable to expect that the concentration of stress visible near the solid surface is due to shear, whereas extensional stress is dominant at the free surface which is literally pulled by the moving plate.

To our knowledge, this is the first experimental evidence of elastic stress boundary layers in extensional flows. This feature of the flow is particularly appealing since it suggests a simplified treatment of our settling sphere problem, in which the stress boundary layer is approximated as an anisotropic elastic membrane.

4. Stability of an axisymmetric membrane in a pressure reservoir

A sphere falling through the free surface of a viscous Newtonian fluid will draw out a funnel-shaped interface similar to what is reported here, and at low Reynolds number *Re* one could reasonably neglect flow effects and solve for the interface shape as a balance between hydrostatic pressure and surface tension. This is essentially the problem of Taylor & Michael (1973), who studied axisymmetric holes in films of Newtonian liquids lying on horizontal surfaces. As the flow in our non-Newtonian fluid is slow ($Re \sim 10^{-3}$), we propose a simple model based on the same principle, taking into account the strong extensional stretching near the free surface in terms of stress boundary layers. While it would of course be more correct to solve the full equations of motion for the fluid, including an appropriate constitutive equation, we hope to gain some understanding of the instability which leads to surface folds using this simplified but more tractable model.

For a Deborah number of 1, elastic effects are very important, especially in a transient extensional flow like ours. Since we have reasonable evidence of the existence of interfacial stress boundary layers in extensional flows, we will model the main features of the interface shape and its instability by assuming that the fluid is divided in two regions: an interfacial zone which behaves essentially as an elastic membrane (of thickness w) stretched by the moving sphere, and an almost static fluid in the bulk where the flow is negligible. The relaxation of the fluid is neglected on the timescale of the experiment: the onset of instability is reached within a few seconds, whereas $\lambda \simeq 6$ s. Under this assumption, the deformation of the interface can be considered as a succession of quasi-static equilibrium states, where the tension in the membrane

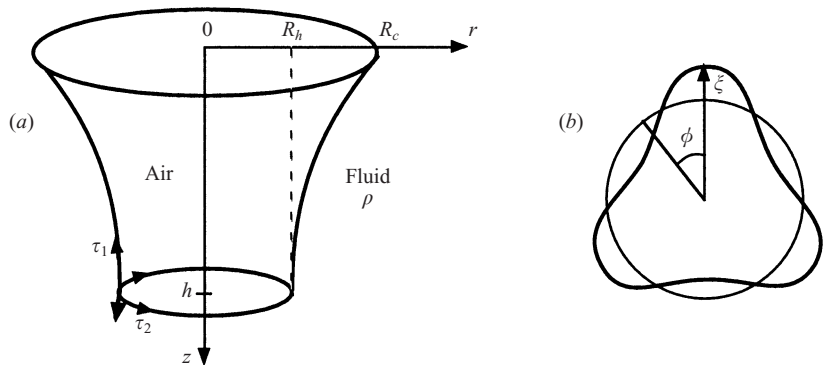

FIGURE 7. (*a*) Notation for the model. The elastic membrane is axisymmetric with respect to the z-axis. The fluid is outside (density ρ), with flat free surface at $z = 0$ and air is inside. The radii of the membrane at $z = 0$ and $z = h$ are fixed and respectively equal to R_c and R_h. (*b*) Cross section at $z = h$ in the perturbed state.

balances hydrostatic pressure. In other words, we assume that there is a separation of timescales between the slow extensional flow which creates the interfacial elastic stress and the force balance which acts to determine the shape of the interface. Kumar & Graham (2000) investigated numerically the similar case of an initially conical elastic (neo-Hookean) membrane enclosing a constant volume of fluid, and showed that it was unstable with respect to azimuthal perturbations. In this section, we represent our flow as an elastic membrane separating a reservoir of fluid from an axisymmetric hole, as sketched in figure 7, and we address its linear stability. Note that, because the streamlines of the flow due to the settling sphere are along the meridians of the interface, we expect that the tension in the membrane approximation will be anisotropic, and much larger along the streamlines.

4.1. *Base state*

We define τ_1 and τ_2 as the stresses along the principal directions integrated over the thickness w of the membrane; $\tau_1(z,t)$ and $\tau_2(z,t)$ are thus the stress resultants in the direction of meridian curves and curves of latitude, respectively, at a given position z and time t. The equation of equilibrium for a thin membrane in a hydrostatic pressure field is (Green & Adkins 1960)

$$\rho g z = \tau_1(z,t)\frac{r''(z)}{(1+(r'(z))^2)^{3/2}} - \tau_2(z,t)\frac{1}{r(1+(r'(z))^2)^{1/2}}, \tag{4.1}$$

where ρ is the density of the fluid, g the acceleration due to gravity, and r the distance to the vertical symmetry axis.

These stress resultants are functions of the local extension ratios which depend on the global deformation of the membrane. They can be related to strains using the equations of finite elasticity for axisymmetric membranes (Green & Adkins 1960), with a simple elastic constitutive equation like the neo-Hookean model:

$$\tau_1 = 4Cw\lambda_3(\lambda_1^2 - \lambda_3^2), \tag{4.2}$$

$$\tau_2 = 4Cw\lambda_3(\lambda_2^2 - \lambda_3^2), \tag{4.3}$$

where λ_1 and λ_2 are the extension ratios in the principal directions of the membrane and $\lambda_3 = (\lambda_1\lambda_2)^{-1}$.

It is in principle possible to obtain the exact equilibrium shape of the interface by solving equations (4.1)–(4.3) along with the internal equilibrium condition:

$$\frac{\mathrm{d}}{\mathrm{d}s}(\tau_1 r) = \tau_2 \frac{\mathrm{d}r}{\mathrm{d}s}, \tag{4.4}$$

where s is the arclength along the meridian curves. However, in the general case, no analytical solution is known, and numerical simulation is probably necessary.

Equation (4.1) is a generalization of the equation for constant-curvature problems. If we set $\tau_1 = \tau_2 = \sigma$ (surface tension) and $\rho = 0$ (no fluid on both sides), we get the classical minimal surface equation (e.g. for soap films), where the solution is a surface of zero mean curvature. This solution (a catenoid) collapses and pinches off symmetrically if the height of the soap film is too large compared to its diameter (Chen & Steen 1997). If we set $\tau_1 = \tau_2 = \sigma$ and $\rho \neq 0$, we obtain the same equation as Taylor & Michael (1973). In this case, there exists a critical thickness of the fluid of order the capillary length, above which no static solution exists. Below this critical value, there is a single solution for each value of the total depth h.

In the elastic membrane approximation, we implicitly assume for simplicity that τ_1 and τ_2 are nearly constant (z-independent) in some region of the interface. We thus treat them as parameters, and do not seek to relate them to strains in the membrane. This is equivalent to solving the equilibrium problem in equation (4.1) for a given position (fixed t) of the sphere. One can then define a characteristic length $\ell = (\tau_1/\rho g)^{1/2}$, the analogue of the capillary length in Newtonian interfacial problems. Rescaling all lengths by ℓ and restricting the analysis to the waist where the instability is more likely to occur because the curvature is highest, we have $r'(z) \ll 1$ and the force balance equation (4.1) becomes

$$r''(z) - \beta r^{-1} - z = 0, \tag{4.5}$$

where $\beta = \tau_2/\tau_1$ is the only non-dimensional parameter.

We seek to demonstrate the existence of an instability occurring when both ends of the membrane are sufficiently pulled apart; we will not attempt to compute the exact solution $r(z)$ for equation (4.5). Since the experiment shows that the meridians of the membrane are approximately parabolic around $z = h$, we assume

$$r(z) \simeq R_h + (R_c - R_h)h^{-2}(z - h)^2. \tag{4.6}$$

This is equivalent to a Taylor expansion of order 2 around $z = h$, where R_h is the minimum radius of the hole, and R_c is the effective radius at $z = 0$. Evaluating the force balance (4.5) at $z = h$ gives an equilibrium condition relating h, R_h and R_c for the axisymmetric interface:

$$2(R_c - R_h)h^{-2} - \beta R_h^{-1} - h = 0. \tag{4.7}$$

4.2. *Linear stability*

To assess the stability near the narrow waist of the membrane (4.6), we will simply assume a small periodic distortion of its shape, and calculate whether the forces arising in the membrane will enhance or diminish it. We assume the perturbed membrane at $z = h$ is of the form

$$r_p(h, \phi) = R_h(1 + \xi \cos n\phi), \tag{4.8}$$

where n is the order of the perturbation mode, ϕ the azimuthal, angle and ξ the relative amplitude of the perturbation (see figure 7*b*). If the perturbation is sufficiently

small, meridians are still parabolic, so that we can write

$$r_p(z,\phi) = r_p(h,\phi) + (R_c - r_p(h,\phi))(z-h)^2 h^{-2}. \tag{4.9}$$

Note that in equations (4.1) and (4.5), we only considered the elastic stresses arising from the stretching of the membrane. The extension ratios in our problem being rather large (of order 1), the bending energy is probably negligible in the base state for a thin membrane. Moreover, the unstressed state will not be the initially flat fluid surface, at which point the polymers are unstretched, but at some later time, when the surface is already funnel shaped.

In the perturbed state however, the particular form we choose for the perturbation induces significant bending of the membrane, whereas it does not introduce any additional stretching effect: at first order, the perimeter of the equator (waist) is constant. Thus we believe that the bending forces will play an important role in the perturbed force balance, whereas almost no additional stretching will occur, i.e. τ_1 and τ_2 will not be modified by the perturbation (at least at leading order). Consequently, only the curvature terms should be modified in equation (4.7) due to the change in geometry, β being kept constant. Then we will add a bending force in an *ad hoc* way, to introduce a damping term in the equation and qualitatively capture the effect of this force.

In the limit $w << R_h$, we use the classical equation of equilibrium relating the deformation ζ of an incompressible plate to the external force distribution P acting on it (Landau & Lifshitz 1970):

$$P = (1/9)Ew^3\nabla^4\zeta, \tag{4.10}$$

where E is Young's modulus, $\zeta = R_h\xi\cos n\phi$ and $\nabla = R_h^{-1}\partial/\partial\phi$. Strictly speaking, this equation is only valid for small deformations, whereas our membrane is already highly stretched. However, we will assume the validity of equation (4.10) to represent influence of bending forces on the stability. Thus, the bending force *exerted by the membrane* is

$$F_b = -\frac{E^* w^3 n^4}{9R_h^3}\xi\cos n\phi, \tag{4.11}$$

where $E^* = E/\rho g\ell$ is the non-dimensional modulus, and all lengths are rescaled by ℓ.

The contribution of τ_1 represented by the first term in equation (4.7) becomes

$$F_1 = 2h^{-2}(R_c - R_h(1+\xi\cos n\phi)). \tag{4.12}$$

The curvature in the horizontal plane of the perturbed membrane at $z = h$ is

$$\kappa = \left(r_p^2 + 2(\partial r_p/\partial\phi)^2 - r_p(\partial^2 r_p/\partial\phi^2)\right)\left(r_p^2 + (\partial r_p/\partial\phi)^2\right)^{-3/2}. \tag{4.13}$$

Expanding κ in powers of ξ and neglecting terms of order higher than one, we obtain the following expression for the τ_2 term:

$$F_2 = -\beta R_h^{-1}(1 + (n^2-1)\xi\cos n\phi). \tag{4.14}$$

The driving force of the instability F is the sum of all forces acting on the membrane in the perturbed case: $F = F_1 + F_2 + F_b - h$. Subtracting the equilibrium condition in the unperturbed state (equation (4.7)), we obtain the following expression for F:

$$F = -\left(\frac{2R_h^2}{h^2} + \beta(n^2-1) + \frac{E^* w^3 n^4}{9R_h^2}\right)\xi\cos n\phi. \tag{4.15}$$

This force is destabilizing if its sign is identical to that of the perturbation $\xi\cos n\phi$, or

$$\alpha(n^2-1)-\delta n^4-1\geqslant 0, \tag{4.16}$$

where $\alpha=-\beta h^2/(2R_h^2)$ is a control parameter known from experiments to increase as the sphere sinks, and $\delta=Ew^3h^2/(18\rho gR_h^4)$ represents the relative importance of the stabilizing effect due to bending (all quantities are dimensional here). At the onset of instability, this force is exactly zero and $\alpha=\alpha_c$.

4.3. *Discussion*

For a Newtonian fluid, $\beta=1$ ($\tau_1=\tau_2=\sigma$), and $\delta=0$ (since $w=0$), so that the instability criterion (4.16) reduces to

$$1+\frac{h^2}{2R_h^2}(n^2-1)\leqslant 0. \tag{4.17}$$

There is no solution except when $n=0$, which corresponds to an axisymmetric expansion/contraction of the interface. Consistent with experimental observation, the system is always stable with respect to azimuthal disturbances.

In contrast, if the membrane models a stretched viscoelastic interface, the tension in the membrane has both a surface tension and an elastic component which can be dominant if the deformations are large. As the moving sphere sinks in the fluid, the interface is stretched in the meridian direction and a positive τ_1 builds up. On the other hand, the fluid motion can pull a region of the surface at a given diameter on the interface to a smaller diameter, which may cause the azimuthal component τ_2 (hoop stress) to become negative. Kumar & Graham (2000) showed that a converging extensional flow near a free surface produces such a compressive stress. In the membrane approach, such a negative or compressive tension is also seen in the study of a membrane enclosing a constant volume of fluid (Kumar & Graham 2000). In equation (4.3), the condition $\tau_2<0$ translates into $\lambda_2<\lambda_3$ or $\lambda_1\lambda_2^2<1$. If we assume a large deformation in which the length of the meridian curve is multiplied by say 2, and the distance to the axis of some material point is reduced to half its original value, then we have $\lambda_1=2$, $\lambda_2^2=1/4$, which gives $\tau_2<0$. This would be likely to occur at a point when the meridian line is sufficiently curved, and R_h is small compared to the overall size.

Thus β may become negative, and α positive which allows one or more unstable modes of deformation. A given mode n becomes unstable at

$$\alpha_c=(1+\delta n^4)/(n^2-1). \tag{4.18}$$

The most unstable mode $\tilde{n}$ corresponds to $\partial\alpha_c/\partial n=0$, that is

$$\tilde{n}=\left(1+(1+\delta^{-1})^{1/2}\right)^{1/2}. \tag{4.19}$$

If we neglect the bending of the membrane ($\delta\to 0$) then $\tilde{n}\to\infty$, i.e. higher-order modes are more unstable than lower ones. In this case, the tension τ_2 acts like a *negative surface tension*, which promotes surface creation and high curvatures. This feature is essential since it gives rise to an entire new class of instabilities unseen in Newtonian fluids where surface tension is positive. If we consider a finite thickness w for the membrane, $\delta>0$ and $\tilde{n}$ is a decreasing function of δ. For sufficiently large values of δ, the onset of instability for the lowest-order modes is reached first (figure 8). Experimentally, with axisymmetric boundary con-

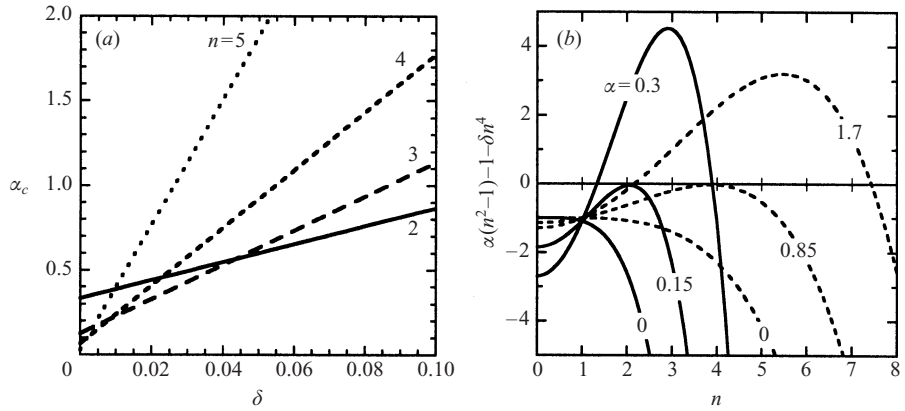

FIGURE 8. (*a*) Value of the control parameter α_c at the onset of instability versus the bending parameter δ, for different modes of instability n. When the bending effect is negligible (δ small), high-order modes are more unstable. Above $\delta \simeq 0.05$, the simplest mode $n = 2$ is the most unstable. (*b*) Rescaled driving force $\alpha(n^2-1)-1-\delta n^4$ versus instability mode n for $\delta = 0.005$ (dotted curves) and $\delta = 0.1$ (solid curves), and increasing values of the control parameter α.

ditions, we observed almost exclusively modes $n = 2$ and 3, which corresponds to $\delta \simeq 0.05$.

5. Conclusion

We have presented a new experiment in which the behaviour of a viscoelastic fluid departs strikingly from that of a Newtonian fluid. As a rigid sphere slowly sinks through the free surface of the fluid, the interface shape undergoes symmetry breaking and pinches in a non-axisymmetric way, leaving creases on the surface. We suggest a simplified model to provide a mechanism of instability for the genesis of these surface folds.

Although modelling the interface as an anisotropic elastic membrane bounding a static fluid is a crude simplification of the physical system, it provides an interpretation of the instability. We identify this phenomenon as a buckling instability, which requires a strong elasticity of the fluid. This simplified model is in qualitative agreement with experimental observations. Quantitative predictions would require a more realistic model which would take into account the full dynamics of the non-Newtonian fluid.

Finally, we would like to point out the similarity between this surface folding process and the formation of cusps at the trailing end of bubbles rising in non-Newtonian fluids, which is still an unresolved issue. We believe that a mechanism qualitatively similar to that described in this paper is responsible for the nature of the two-dimensional cusp on rising bubbles, a point first raised by Kumar & Grahm (2000). Although the details of the flow are different, the main ingredients of this instability are an elongation in the direction of motion and a contraction in the radial direction responsible for a compressive hoop stress.

We would like to thank J. T. Jacobsen and A. Jayaraman for valuable discussions and critical reading of the manuscript. A. B. acknowledges support from the A. P. Sloan Foundation and National Science Foundation (CAREER Award DMR-0094167). T. P. thanks the Délégation Générale pous l'Armement (French Ministry of Defence) for financial support.

REFERENCES

Bird, R. B., Armstrong, R. C. & Hassager, O. 1987 *Dynamics of Polymeric Liquids*, 2nd edn., vol. 1. Wiley-Interscience.

Chen, Y.-J. & Steen, P. H. 1997 Dynamics of inviscid capillary breakup: collapse and pinchoff of a film bridge. *J. Fluid Mech.* **341**, 245–267.

Green, A. E. & Adkins, J. E. 1960 *Large Elastic Deformations.* Oxford University Press.

Groisman, A. & Steinberg, V. 2000 Elastic turbulence in a polymer solution flow. *Nature* **405**, 53–55.

Hassager, O. 1979 Negative wake behind bubbles in non-Newtonian liquids. *Nature* **279**, 402–403.

Hu, Y., Wang, S. Q. & Jamieson, A. M. 1993 Rheological and flow birefringence studies of a shear-thickening complex fluid – a surfactant model system. *J. Rheol.* **37**, 531–546.

Jeong, J. T. & Moffatt, H. K. 1992 Free-surface cusps associated with flow at low Reynolds number. *J. Fluid Mech.* **241**, 1–22.

Kumar, K. A. & Graham, M. D. 2000 Buckling instabilities in models of viscoelastic free surface flows. *J. Non-Newtonian Fluid Mech.* **89**, 337–351.

Landau, L. D. & Lifshitz, E. M. 1970 *Theory of Elasticity*, 2nd edn. Pergamon Press.

Liu, Y., Liao, T. & Joseph, D. D. 1995 A two-dimensional cusp at the trailing edge of an air bubble rising in a viscoelastic liquid. *J. Fluid Mech.* **304**, 321–342.

Rasmussen, H. K. & Hassager, O. 1999 Three-dimensional simulations of viscoelastic instability in polymeric filaments. *J. Non-Newtonian Fluid Mech.* **82**, 189–202.

Rehage, H. & Hoffmann, H. 1991 Viscoelastic surfactant solutions: model systems for rheological research. *Molecular Phys.* **74**, 933–973.

Spiegelberg, S. H. & McKinley, G. H. 1996 Stress relaxation and elastic decohesion of viscoelastic polymer solutions in extensional flow. *J. Non-Newtonian Fluid Mech.* **67**, 49–76.

Taylor, G. I. & Michael, D. H. 1973 On making holes in a sheet of fluid. *J. Fluid Mech.* **58**, 625–639.

Yao, M. & McKinley, G. H. 1998 Numerical simulations if extensional deformations of viscoelastic liquid bridges in filament stretching devices. *J. Non-Newtonian Fluid Mech.* **74**, 47–88.